Journal of Solid State Chemistry 292 (2020) 121712

Contents lists available at ScienceDirect

Journal of Solid State Chemistry

journal homepage: www.elsevier.com/locate/jssc

Synthesis, characterization and catalytic performance of nanocrystalline Co_3O_4 towards propane combustion: Effects of small molecular carboxylic acids

Zhao Liu [a,b], Lijun Cheng [a,b], Jia Zeng [a,b], Xin Hu [a,b], Shiyun Zhangxue [a,b], Shanliang Yuan [a], Qifei Bo [a], Biao Zhang [a,**], Yi Jiang [a,*]

[a] National Engineering Laboratory for VOCs Pollution Control Material & Technology (Chengdu), Chengdu Institute of Organic Chemistry, Chinese Academy of Sciences, Chengdu, 610041, Sichuan, China

[b] University of Chinese Academy of Sciences, Beijing, 100049, China

ARTICLE INFO

Keywords:
Co_3O_4
Small molecular carboxylic acids
Complexing agent
Catalytic combustion
Propane

ABSTRACT

A series of nanocrystalline Co_3O_4 catalysts were synthesized by low-temperature liquid phase complexation with different small molecular carboxylic acids (citric acid, oxalic acid, and tartaric acid). The effects of different carboxylic acids on the catalyst structure and surface microenvironment were discussed in detail, and the catalytic performance of propane combustion was investigated. The results showed that different carboxylic acids changed the distance between Co^{2+} ions in the catalyst precursor, which directly affected the crystallite size (12–16 nm) and specific surface area (10~31 $m^2\ g^{-1}$) of nanocrystalline Co_3O_4. Among them, Co_3O_4 synthesized from the cobalt citrate precursor with the largest Co^{2+} ion distance has the best catalytic activity. The conversion rate of propane reached 90% at 250 °C and showed stable performance in 40 h continuous reactions. The excellent catalytic performance could be allocated to the smallest crystallite size, excellent texture properties, a high degree of lattice disorder, unique surface composition, and excellent reducibility.

1. Introduction

Volatile organic compounds (VOCs) emitted by human production activities have become the main pollutants in the atmosphere and contribute significantly to the formation of photochemical smog, ozone, and greenhouse gases [1,2]. Among them, short-chain alkanes from $C_{2\text{-}4}$ are the most challenging species to eliminate due to their high activation energy and stability of C-C and C-H bonds. Compared with other VOCs treatment technologies, catalytic combustion has high VOCs removal efficiency and harmless products H_2O and CO_2 at relatively low temperature, which is extremely effective for VOCs control and emission reduction [3].

The focus of the development of VOCs catalytic combustion technology is the design and preparation of high-performance catalysts. Researchers have conducted extensive studies on noble metal-based catalysts (Pt [4], Pd [5], Ru [6,7], etc.) and found that they are effective catalysts for the complete oxidation of short-chain alkanes, but their application is limited due to their high price and short service life. Hence, the development of inexpensive and highly active non-noble metal oxide catalysts has practical significance. Recently, researchers have explored non-noble metal oxide catalysts such as CoO_x [8,9], MnO_x [10,11], CeO_x [12], NiO_x [13] and corresponding mixtures [14–17] for catalytic combustion of short-chain alkanes, in which single nanocrystalline Co_3O_4 has better catalytic activity [9,18,19]. The activity of Co_3O_4 depends on its specific surface area, crystal size, reducibility, surface oxygen content, morphology, and crystal plane [20–23]. Meanwhile, the preparation method also makes a significant influence on the physical and chemical properties of Co_3O_4. Several methods for preparing Co_3O_4 have been suggested: precipitation [1,24], hydrothermal [21,25], hard template [26,27], combustion [28], sol gel [29] and complex method [30]. Among them, the complex method for preparing nano-oxides has the advantages of high product purity, low heat treatment temperature, and short preparation time.

The study found that complexing agents play a key role in controlling the pore structure and morphology of metal oxides. For example, Yang [31] et al. synthesized 3D micro/nanostructure CeO_2 by changing the

* Corresponding author.
** Corresponding author.
E-mail address: yjiang@cioc.ac.cn (Y. Jiang).

https://doi.org/10.1016/j.jssc.2020.121712
Received 25 July 2020; Received in revised form 30 August 2020; Accepted 4 September 2020
Available online 9 September 2020

types of organic acids (acetic acid, propionic acid, n-butyric acid, and oleic acid), and found that CeO_2 synthesized with acetic acid displayed hierarchical porosity and optimal toluene combustion active. Ren [32] et al. used tartaric acid as the complexing agent and introduced a small amount of nitric acid to adjust the gelation rate of $LaMnO_3$ colloid, to successfully construct $LaMnO_3$ with 3DOM structure, showing good activity in the catalytic oxidation of ethyl acetate. Besides, citric acid has been widely used as a complexing agent to prepare metal oxides and applied to the catalytic combustion of VOCs [19,24,33]. For example, Zhang [34] et al. successfully prepared nanocrystalline $CuMn_2O_4$ oxide with an abundant porous structure using citric acid, which exhibited excellent catalytic performance in the catalytic oxidation of benzene. However, due to the similar structure of many small molecule carboxylic acids with citric acid, the effects of different carboxylic acids on the composition, structure, morphology, and catalytic performance of metal oxide catalysts are rarely mentioned. To our knowledge, the effect of small molecular carboxylic acid on the catalytic performance of Co_3O_4 in the catalytic combustion of short-chain alkanes has not been reported.

In this work, three different small molecular carboxylic acids, citric acid (CA), oxalic acid (OA), and tartaric acid (TA), were used to assist the synthesis of nanocrystalline Co_3O_4. The effects of carboxylic acids on the physicochemical properties of nanocrystalline Co_3O_4 were studied by FT-IR, XRD, BET, XPS, TEM/HRTEM, H_2-TPR and O_2-TPD, and their catalytic performance in catalytic combustion of propane (a typical short-chain alkane) was evaluated. The purpose of this work is to study the effect of different small molecular carboxylic acid on the catalytic activity of Co_3O_4 for propane combustion and systematically discuss the structure-activity relationship between Co_3O_4 and propane conversion.

2. Experimental

2.1. Catalyst preparation

The preparation process of the Co_3O_4 catalyst was similar to the literature [24]. In a typical synthesis process, 0.0274 mol of CA, OA, and TA were added to 25 ml of 1 mol/L $Co(NO_3)_2 \bullet 6H_2O$ aqueous solution under stirring, respectively. The obtained solution was continuously stirred and evaporated at 80 °C for 90 min and dried at 120 °C for 6 h to obtain the corresponding precursor. Then the precursor was calcined in an air atmosphere at 300 °C for 1 h at a heating rate of 2 °C/min to decompose the organic framework [35]. Finally, the corresponding catalysts were obtained by heating to 400 °C at the same heating rate for 2 h and labeled as Co-CA, Co-OA, and Co-TA, respectively.

2.2. Catalyst characterization

Fourier-transform infrared (FT-IR) spectrum was identified from 400 to 4000 cm^{-1} on a Nicolet 6700 FT-IR spectrometer (ThermoFisher, USA). The N_2 adsorption-desorption analyses were measured on a NOVA 2200E nitrogen adsorption instrument (Quantachrome, USA) at −196 °C. Before testing, the catalysts were degassed under vacuum at 300 °C for 3 h. The specific surface areas and pore size distributions were determined by the Brunauer-Emmett-Teller (BET) and Barrett–Joyner–Halenda (BJH) method, respectively. X-ray diffraction (XRD) was determined by a diffractometer (Shimadzu, Japan) with Cu Kα radiation (λ = 0.1541 nm) operated at 40 kV and 30 mA. The scan rate and step sizes were 4 °C/min and 0.02°, respectively. The transmission electron microscope (TEM/HRTEM) was completed by the Tecnai G2 F20 electron microscope (FEI, USA) at an acceleration voltage of 200 kV. X-ray photoelectron spectroscopy (XPS) was performed by the XSAM800 spectrometer (Kratos, USA) using Al Kα radiation (1253.6 eV). The electron binding energy was calibrated based on the C 1s spectrum (284.8 eV). The hydrogen temperature-programmed reduction (H_2-TPR) device consists of a temperature-programmed unit and a thermal conductivity detector (TCD). In the experiment, 15 mg of the catalyst was put into the constant temperature section of the U-shaped quartz tube and pretreated at 300 °C for 1 h under high purity N_2. After cooling to room temperature, the gas was switched to a 5% H_2–95% N_2 mixture at a flow rate of 25 ml/min. The TCD signal was recorded at 10 °C/min from room temperature to 600 °C after the baseline was stable. The H_2 consumption of all catalysts was calibrated by the H_2-TPR treatment of CuO powder. The oxygen temperature program desorption (O_2-TPD) device is the same as H_2-TPR. In each test, 100 mg of the catalyst was placed in a U-shaped quartz tube and pretreated in high purity O_2 at 300 °C for 1 h. After cooling to room temperature, the gas was switched to high purity He at a flow rate of 30 ml/min. The TCD signal was recorded at 10 °C/min from room temperature to 600 °C after the baseline was stable. During the H_2-TPR and O_2-TPD tests, the two ends of the U-shaped tube are connected to a dryer equipped with a color-changing silica gel to eliminate the effect of water vapor.

2.3. Catalytic tests

The catalytic combustion reaction of propane was carried out on a CGK-5A fixed bed reactor with an inner diameter of 8 mm. The propane concentration before and after the reaction was analyzed online using an SC-8000 gas chromatograph equipped with a flame ionization detector (FID), while the CO and CO_2 concentrations from reaction tail gas were measured using an SC-3000 gas chromatograph equipped with a thermal capture detector (TCD). The composition of the raw gas was 0.3 vol % propane balanced by air. The flow rate and catalyst loadings were 100 mL/min and 200 mg, respectively, corresponding to a gas hourly space velocity (GHSV) of 30000 $ml \bullet g^{-1} \bullet h^{-1}$. The conversion of propane is based on equation (1):

$$Y(C_3H_8) = (1 - (C_3H_8)_{out} / (C_3H_8)_{in}) \times 100\% \quad (1)$$

Where $Y(C_3H_8)$ is the conversion of propane, $(C_3H_8)_{in}$ and $(C_3H_8)_{out}$ represents the volume concentration of propane before and after the reaction, respectively.

2.4. Reaction kinetics testing

Kinetic experiments are similar to reported in the literature [36]. Before the experiment, the effect of internal and external diffusion was excluded. The conversion of propane is controlled below 15%, and the reaction rate (r, mol/(s·g)) can be expressed by equation (2):

$$r = N(C_3H_8) \times Y(C_3H_8)/W(Cat) \quad (2)$$

Where $N(C_3H_8)$ is the flow rate of propane (mol/s) and W(Cat) is the mass of the catalyst (g). The process of propane oxidation is irreversible, and the effects of reaction products H_2O and CO_2 on the reaction rate can be ignored. Thus, the reaction rate equation can also be expressed by the Arrhenius equation (3):

$$r = A\exp(-E_a / RT) P^a_{C_3H_8} P^b_{O_2} \quad (3)$$

Where T (K) is the reaction temperature, R is the ideal gas constant (8.314 J/(mol·K)), Ea (kJ/mol) is the apparent activation energy, and A is the pre-exponential factor. During the test, when the propane conversion rate is less than 15%, the composition of the raw gas is approximately constant. The relationship between ln r and RT can be obtained by equation (4):

$$\ln r = -E_a/RT + C \quad (4)$$

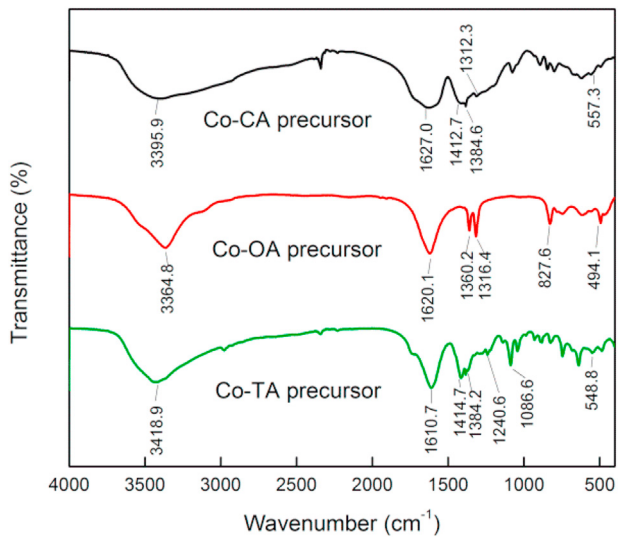

Fig. 1. FT-IR spectrum of different Co_3O_4 precursor in the range of 400–4000 cm^{-1}.

C stands for a constant. By calculating the r at a different temperature, the Ea can be obtained by the slope of the ln r and 1/RT curves.

3. Results and discussion

3.1. FT-IR results

The molecular structure of the Co_3O_4 precursor was revealed by the FT-IR spectrum. As shown in Fig. 1, the absorption peaks of Co-CA precursor, Co-OA precursor, and Co-TA precursor at 557.3 cm^{-1}, 494.1 cm^{-1}, and 548.8 cm^{-1}, respectively, belong to the ν(Co–O) stretching vibration, indicating that the corresponding carboxylic acid is coordinated with Co^{2+} ion.

The absorption peak of the Co-CA precursor at 3395.9 cm^{-1} is attributed to the ν(O-H) stretching vibration peak in the water molecule or OH ligand. The peak at 1627.0 cm^{-1} is ascribed to the ν_{as}(C=O) antisymmetric stretching vibration of the carboxylate group in the coordinated citrate. Moreover, absorption peaks at 1412.7 cm^{-1} and 1384.6 cm^{-1} can be attributed to the ν_s(C=O) symmetric stretching vibration of the carboxylate group. And the difference between the wavenumber of the ν_{as}(C=O) and ν_s(C=O) is 214.3 cm^{-1}, indicating that the carboxyl oxygen participates in the coordination in the form of monodentate [37]. The absorption peak at 1312.3 cm^{-1} is the δ(C-OH) deformation vibration mode, indicating that the hydroxyl in CA does not participate in the complexation of cobalt.

The strong peak of the Co-OA precursor at 3364.8 cm^{-1} is allocated to the stretching vibration of the (O-H) group, indicating the water of hydration. The band at 1620.1 cm^{-1} corresponding to asymmetric ν_{as}(C–O) and the closely spaced bands at 1360.2 cm^{-1} and 1316.4 cm^{-1} assigned to symmetric ν_s(C–O), respectively, clearly reveal the presence of bridging oxalates, with all four oxygen atoms coordinated to the cobalt atoms [38,39]. The peak at 827.6 cm^{-1} is assigned to the δ(O–C–O) band appears [38].

For the Co-TA precursor, the strong and broad peak at 3418.9 cm^{-1} is attributed to the ν(O-H) stretching mode, indicating the presence of water of hydration or OH ligand [40]. The sharp peaks at 1610.7 and 1414.7 cm^{-1} are attributed to the ν_{as}(C=O) asymmetric stretching vibration and the ν_s(C=O) symmetric stretching vibration of the carbonyl groups. Close to 1414.7 cm^{-1}, the weak peak at 1384.2 cm^{-1} is also caused by the ν_s(C=O) symmetric stretching. The absorption peak at 1240.6 cm^{-1} is assigned to the out of plane bending vibration mode of δ(C-OH), indicating that the alcohol hydroxyl is not dissociated [41]. These results indicate that TA and Co^{2+} are mainly coordinated in the form of bidentate. The strong peak at 1086.6 cm^{-1} is attributed to δ(C–H) deformation vibration as well as π(C–H) skeleton vibration mode.

FTIR shows that small molecular carboxylic acids and Co^{2+} in the precursor have different binding modes. And the possible coordination forms of different precursors are shown in Fig. 2. Among them, the hydroxyl group in CA and TA did not coordinate, while the CA, OA, and TA coordinate with Co^{2+} in the form of monodentate, tetradentate, and bidentate, respectively. Due to the coordination of CA with Co^{2+} in the form of monodentate, the distance between Co^{2+} is relatively long. Meanwhile, CA has the longest chain length among all carboxylic acids, which will further expand the distance between Co^{2+} ions and effectively dispersing Co^{2+} ions. OA coordinates with Co^{2+} in the form of tetradentate, resulting in two five-membered rings between Co^{2+}, which is slightly shorter than the distance between Co^{2+} in CA coordination. However, TA coordinates with Co^{2+} in a bidentate form, resulting in only a seven-membered ring between Co^{2+}, which has the shortest distance. Therefore, the distance between Co^{2+} after coordination with carboxylic acids is as follows: Co-CA precursor > Co-OA precursor > Co-TA precursor. The larger the distance between Co^{2+}, the more conducive to the formation of high-dispersion and small crystalline size Co nanoparticles after calcination, which is further confirmed by XRD, N_2 adsorption-desorption, and TEM. It can be inferred that the Co oxide prepared by monodentate coordination with CA can fully contact with propane molecules to enhance the catalytic activity.

3.2. XRD results

The XRD patterns of Co-CA, Co-OA, and Co-TA are shown in Fig. 3. All the catalysts show diffraction peaks at 2θ = 31.2°, 36.8°, 38.6°, 44.8°, 55.6°, 59.3°, 65.2°, corresponding to the (220), (311), (222), (400), (422), (511) and (440) planes of spinel Co_3O_4 (JCPDS 43-1003). Meanwhile, no additional diffraction peaks appeared in all samples, indicating that only pure Co_3O_4 phase exists. Also, the diffraction peak intensity of catalysts is significantly different. Co-CA has the weak and broad diffraction peak, which means small crystalline size and poor crystallinity [42]. The average crystalline size of Co_3O_4 based on (311) plane is calculated by Scherrer equation, and the corresponding results are shown in Table 1. Compared to Co-OA and Co-TA, Co-CA has the smallest crystalline size (11.8 nm), indicating that the addition of CA is conducive to the formation of small crystalline size Co_3O_4.

3.3. N_2 adsorption-desorption results

The N_2 adsorption-desorption isotherms and BJH pore size distributions of nanocrystalline Co_3O_4 are shown in Fig. 4. All catalysts exhibit typical IV shape isotherms with H3-type hysteresis loops at P/Pa>0.75, indicating the existence of mesoporous structure [43]. The relatively broad hysteresis loop in the Co-CA isotherm indicates effective mass transfer and less pore-blockage [44]. The pore size distribution of all catalysts is mainly concentrated at 2∼30 nm, having a center in the range of 17 nm. The mesopores are disordered and may originate from the extrusion between particles. The texture properties are summarized in Table 1. Compared to Co-OA and Co-TA, Co-CA has the largest specific surface area (31.4 $m^2 g^{-1}$) and pore-volume ($5.6*10^{-2}$ cm^3 g), which can effectively enhance the contact area between the catalyst surface and gas-phase molecules [45].

3.4. TEM results

Fig. 5 shows the TEM images and particle size distributions of Co-CA, Co-OA, and Co-TA. All Co_3O_4 are nanoparticles assembled from irregular polyhedrons and have different degrees of aggregation. Among them, the accumulation of small particles in Co-CA and Co-OA produces a large number of mesopores, while the aggregation of larger particles in Co-TA significantly reduces the number of pores, coinciding well with N_2 adsorption-desorption results. And the average particle size of Co-CA

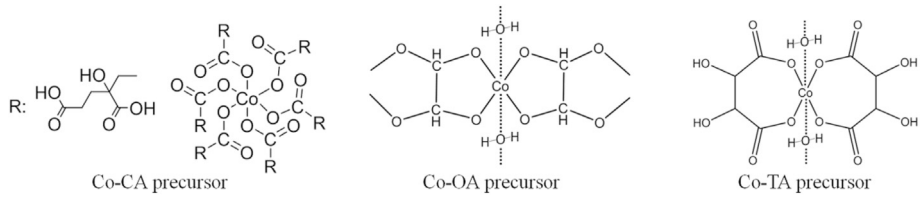

Fig. 2. Possible coordination forms of different Co_3O_4 precursors.

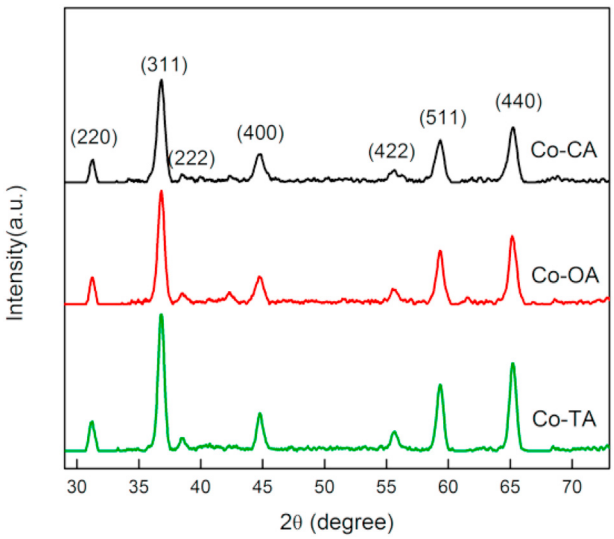

Fig. 3. XRD patterns of Co-CA, Co-OA and Co-TA.

Table 1
Texture properties and crystalline size of Co-CA, Co-OA and Co-TA.

Sample	$S_{BET}(m^2 \cdot g^{-1})$	V_p*10^{-2} (cm^3 g)	D_{BJH}(nm)	[a]Crystalline size (nm)
Co-CA	31.4	5.6	4.0	12.6
Co-OA	17.2	3.7	3.6	14.9
Co-TA	9.9	2.0	3.6	15.7

[a] The crystalline size of Co_3O_4 was calculated based on the (311) plane.

(13.89 nm) is smaller than that of Co-OA (17.37 nm) and Co-TA (23.64 nm), which is in line with XRD results.

3.5. HRTEM results

Fig. 6 presents the HRTEM images of different nanocrystalline Co_3O_4 catalysts. The lattice fringes of Co-CA are messy and unclear, showing poor crystallinity and high lattice disorder, which can be attributed to more crystal defects, whereas Co-OA and Co-TA have higher crystallization degree. Abundant surface defects may provide sufficient active sites for deep oxidation reactions [46], which may contribute the much improved activity in Co-CA over the Co-OA and Co-TA. The lattice fringe spacing of Co-OA and Co-TA is 0.467 nm, corresponding to the (111) crystal plane of Co_3O_4. However, Co-CA exposes lattice fringes with spacing of 0.243 nm and 0.286 nm, which are assigned to (311) and (220) crystal planes of Co_3O_4, respectively. According to the literature [47–49], the (111) crystal plane of Co_3O_4 contains only Co^{2+} ions rather than the active surface, while the (220) crystal plane of Co_3O_4 is mainly composed of Co^{3+} ions, which can contribute enough active sites for VOCs oxidation. Nanocrystalline Co_3O_4 with abundant surface defects and exposed (220) crystal planes may exhibit better catalytic activity in the propane combustion reaction.

3.6. XPS results

The surface composition and oxidation state of catalysts were investigated by XPS technology. Fig. 7(a) shows the Co 2p XPS spectrum of the as-prepared nanocrystalline Co_3O_4. The electrons in the 2p orbital of Co cause spin-orbital splitting, generating two main peaks of Co $2p_{3/2}$ and Co $2p_{1/2}$ near BE of 780.0eV and 795.0eV, and two shake-up satellites peaks near BE of 785.0eV and 803.0eV, which proves the presence of Co_3O_4 [50]. By peak fitting deconvolution technology, the Co $2p_{3/2}$ peak was decomposed into two peaks near BE of 779.5 eV and 781.0 eV, which belongs to the surface Co^{3+} and Co^{2+}, respectively [50–52]. The XPS parameters of catalysts are shown in Table 2. The order of the molar ratio of Co^{3+}/Co^{2+} on the surface of Co_3O_4 from large to small is: Co-CA > Co-OA > Co-TA, indicating more Co^{3+} ions on the surface of Co_3O_4 prepared with CA, while the Co^{3+} ions with lower Co^{3+}-O bond energy are conducive to the release of reactive oxygen species, thus enhancing the catalytic oxidation performance [53].

As shown in Fig. 7(b), the O1s peaks are also classified by peak fitting deconvolution technique. The peaks at 528.9, 529.1 and 529.1eV belong to the lattice oxygen species O_{latt} (O^{2-}), the peaks at 530.5, 530.6 and 530.8eV belong to the surface-adsorbed oxygen species O_{ads} (O_2^{2-}、O_2^-、O^-), the peaks at 532.3, 532.4 and 532.3eV are attributed to molecular

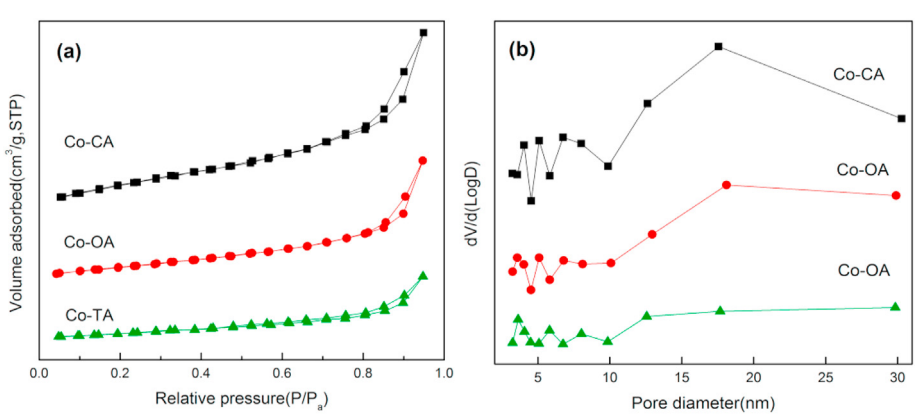

Fig. 4. (a) N_2 adsorption-desorption isotherms; (b) Pore size distribution of Co-CA, Co-OA and Co-TA.

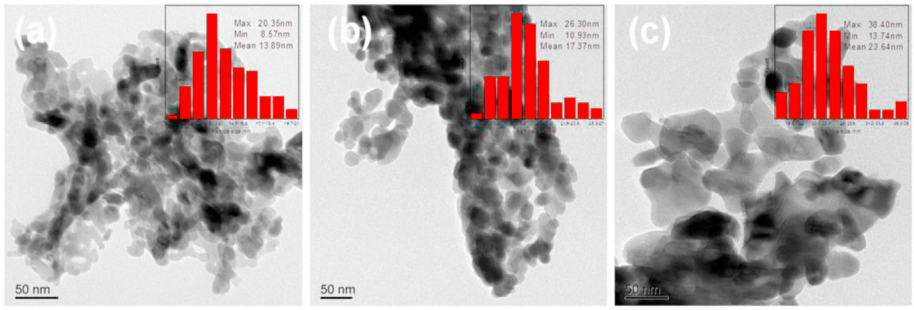

Fig. 5. TEM and particle size distributions of (a) Co-CA; (b) Co-OA; (c) Co-TA.

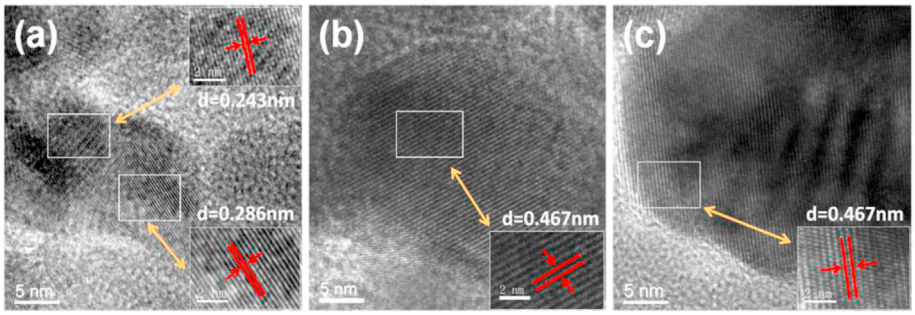

Fig. 6. HRTEM images of (a) Co-CA; (b) Co-OA; (c) Co-TA.

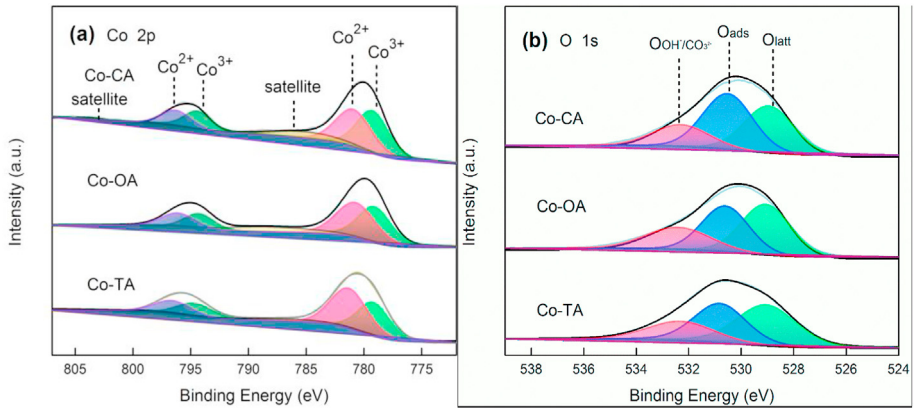

Fig. 7. (a) Co 2p and (b) O 1s XPS spectra of Co-CA, Co-OA and Co-TA.

Table 2
XPS parameters of Co-CA, Co-OA and Co-TA.

Catalyst	Binding energy (eV)					Surface element contents (mol. %)		Co^{3+}/Co^{2+}	O_{ads}/O_{latt}
	Co^{2+}	Co^{3+}	O^{-}_{OH}/O^{2-}_{CO3}	O_{ads}	O_{latt}	Co	O		
Co-CA	781.0	779.2	532.3	530.5	528.9	28.6	71.4	0.99	1.19
Co-OA	780.8	779.1	532.4	530.6	529.1	32.4	67.7	0.84	0.87
Co-TA	781.2	779.2	532.3	530.8	529.1	33.5	66.5	0.72	0.83

water (i.e., hydroxyl) or carbonate species [54,55]. It can be seen from Table 2 that the mole ratio of O_{abs}/O_{latt} on the catalyst surface from high to low is: Co-CA > Co-OA > Co-TA. Generally, the mobility of surface adsorbed oxygen is higher than that of lattice oxygen, and thus more active in oxidation reaction [46]. Therefore, the nanocrystalline Co_3O_4 prepared by CA complexation has more surface Co^{3+} ions and surface adsorbed oxygen species, which will exhibit better activity in catalytic combustion of propane.

3.7. H_2-TPR results

The H_2-TPR profiles of different nanocrystalline Co_3O_4 are shown in Fig. 8. After peak fitting, two partially overlapping reduction peaks (α and β peak) in the center at approximately 340 °C and 400 °C are present, which can be attributed to the reduction of $Co^{3+}\rightarrow Co^{2+}$ and $Co^{2+}\rightarrow Co$ in Co_3O_4, respectively [42,56]. As for the Co-OA and Co-TA, the corresponding reduction peaks shifted to a higher temperature compared with that of the Co-CA, which indicates that the complexing agent strongly

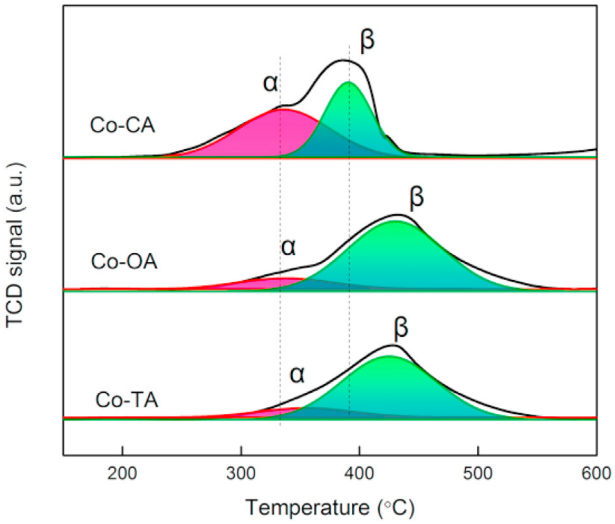

Fig. 8. H_2-TPR of Co-CA, Co-OA and Co-TA.

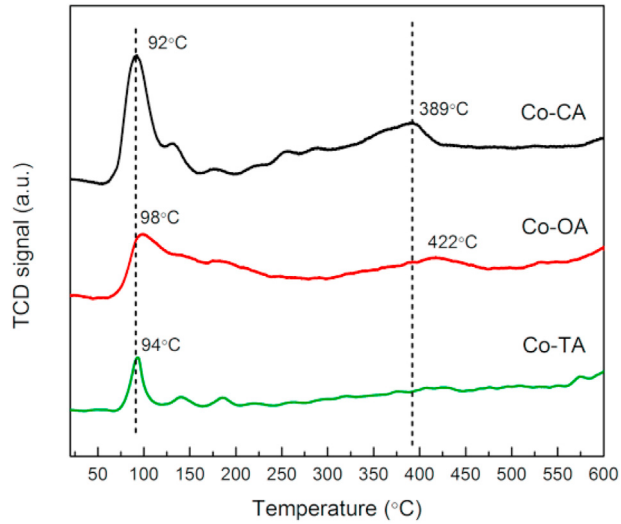

Fig. 9. O_2-TPD of Co-CA, Co-OA and Co-TA.

Table 3
H_2-TPR parameters of the Co-CA, Co-OA and Co-TA.

Catalyst	H_2-TPR			
	Temperature (°C)		H_2 consumption (mmol·g^{-1})	
	α	β	α	β
Co-CA	336	390	6.91	5.34
Co-OA	337	430	1.99	12.51
Co-TA	354	426	1.72	11.57

affected the reducibility of Co_3O_4. The reduction behavior of Co_3O_4 is greatly affected by the particles size and dispersion state of cobalt [56, 57]. As described in XRD and TEM, Co-CA is composed of smaller nanocrystals, which may result in more exposed areas and easier reduction. The nanocrystalline Co_3O_4 prepared using citric acid as complexing agent contained more easily reduced species than that of Co-OA and Co-TA, which is promising for improved catalytic activity for propane combustion. Table 3 summarizes the reduction peak temperature and H_2 consumption of the catalyst. The total theoretical H_2 consumption for the reduction of well-defined Co_3O_4 is 16.6 mmol g^{-1}. However, the total experimental H_2 consumption measured for the different Co_3O_4 catalysts ranged from 12.3 to 14.5 mmol g^{-1}, which is lower than the theoretical H_2 consumption. This difference suggests a proportion of Co^{2+} in the catalysts greater than that indicated by the stoichiometric ratio. Whether it is α peak or β peak, Co-CA has a lower reduction peak temperature than Co-OA and Co-TA, indicating a weaker Co-O bond strength and stronger oxidation performance. Besides, the order of the H_2 consumption of the α peak is: Co-CA > Co-OA > Co-TA, indicating a large number of easily dissociable Co^{3+}-O species on Co-CA involved in the reduction of $Co^{3+}\rightarrow Co^{2+}$, which is consistent with XPS results. Combining HRTEM and XPS analysis shows that nanocrystalline Co_3O_4 prepared by CA complexation has a high degree of lattice disorder, which is conducive to the adsorption of oxygen species and participates in the oxidation reaction as active oxygen, which may be the main reason for the easier reduction of Co-CA.

3.8. O_2-TPD results

Fig. 9 shows the O_2-TPD profiles of Co-CA, Co-OA and Co-TA. In general, the desorption of oxygen species in inert atmosphere is closely related to temperature [19]. Surface adsorbed oxygen species (O_2^-, O^-, O_2^{2-}) are more easily desorbed from transition metal oxides as a surface-active oxygen species and participates in oxidation reactions, and lattice oxygen (O^{2-}) species are difficult to be desorbed due to their strong bond energy [43]. From Fig. 9, all catalysts produced several distinct desorption peaks, corresponding to different oxygen species. The desorption peaks in the regions below 350 °C, between 350 °C and 500 °C and above 500 °C are attributed to the desorption of surface adsorbed oxygen, surface lattice oxygen, and bulk lattice oxygen, respectively [58].

Table 4
Oxygen desorption peak area of catalyst.

Catalyst	The peak areas (<350 °C)	The peak areas (350°C–500 °C)
Co-CA	1578173	331081
Co-OA	1095408	159011
Co-TA	317700	52121

The oxygen desorption peak areas of the catalysts are given in Table 4. In the surface adsorbed oxygen desorption stage (below 350 °C), the oxygen desorption peak area of Co-CA is 1.44 and 4.96 times that of Co-OA and Co-TA, respectively, which can provide more active oxygen in the oxidation reaction species. Combined with N_2 adsorption-desorption and HRTEM analysis, Co-CA with a large specific surface and high lattice disorder will form more heterogeneous, convex, and rough structures, which is conducive to the generation of oxygen vacancies on the surface, thus generating abundant adsorbed oxygen species and improving catalytic oxidation performance. Besides, in the surface lattice oxygen desorption stage (350°C–500 °C), Co-CA still has the largest oxygen desorption peak area, which is 2.08 and 6.35 times that of Co-OA and Co-TA, respectively, indicating its existence more surface lattice oxygen species. When the surface adsorbed oxygen species are consumed, the surface lattice oxygen starts to be activated and participates in the reaction, and the generated oxygen vacancies will further capture gas phase oxygen and form a redox cycle. Furthermore, the lattice oxygen desorption peak temperature of Co-CA is lower than that of Co-OA, indicating a better surface lattice oxygen mobility, which will effectively promote the combination of oxygen species and reactant molecules and the filling of oxygen vacancies, thereby improving catalytic oxidation performance.

3.9. Catalytic activity determination, kinetics study, and stability test

The products of catalytic combustion of propane are shown in Fig. 10. Only propane and CO_2 were detected in the FID and TCD detection systems, and no associated hydrocarbons and CO were detected, indicating that propane was completely oxidized.

The catalytic combustion activity of propane under different nanocrystalline Co_3O_4 is shown in Fig. 11(a). The light-off temperature (T_{10})

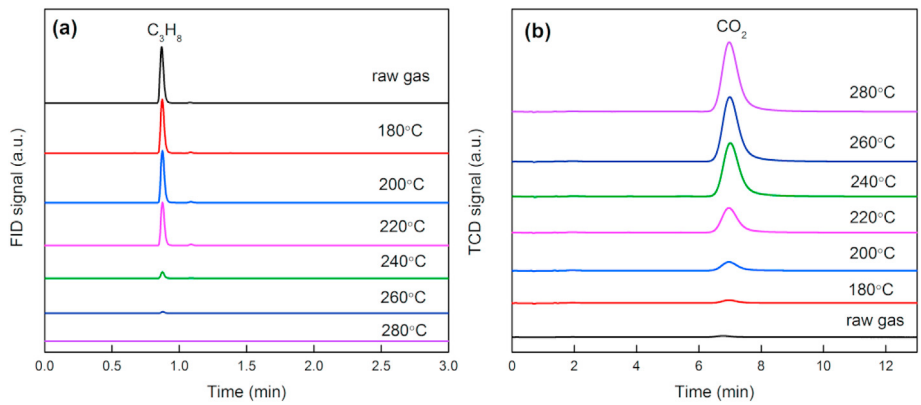

Fig. 10. Composition of reaction products (a) Propane content; (b) CO_2 content. Test conditions: The feed consisted of 0.3 vol% propane balanced by air, with a gas hourly space velocity (GHSV) of 30000 mL/(h·g).

of all catalysts is about 180 °C. As the temperature increases, the conversion rate of propane increases rapidly. With a 90% propane conversion rate (T_{90}) as the activity evaluation criterion, the T_{90} of Co-CA is 250 °C, showing a best low-temperature catalytic activity. However, the T_{90} of Co-OA and Co-TA is 262 °C and 279 °C respectively, which is 12 °C and 29 °C higher than that of Co-CA.

Fig. 11(b) presents the Arrhenius relationship curve between ln r and 1/RT, and the corresponding activation energy (Ea) is obtained from the slope of the fitted straight line. The order of Ea is as follows: Co-TA > Co-OA > Co-CA, where Co-CA has the lowest Ea of 43.9 kJ/mol. The lower Ea has a lower reaction barrier, revealing that the catalytic combustion reaction on Co-CA could be easier to initiate [59].

Although all catalysts are composed of pure Co_3O_4 phase, Fig. 11(c) shows that the activity of the catalyst has a certain dependence with the crystalline size. It can be clearly seen that the larger crystalline size corresponds to higher T_{50} and T_{90} temperatures, while Co-CA has the smallest crystalline size (12.6 nm), corresponding to the optimal catalytic propane conversion activity. The small size effect of this nanocrystalline Co_3O_4 is similar to the work of Rivas [60].

The catalytic performance with time on the line of the Co-CA is displayed in Fig. 11(d). After 40 h of operation at 250 °C, the conversion rate of propane is maintained at about 90%, indicating that Co-CA has good stability.

The activity of the Co-CA was compared to that reported in the literature, as shown in Table 5. In this work, the catalytic activity of Co-CA can be comparable to other Co_3O_4, two-component transition metal oxides, rare earth catalysts as well as noble metal catalysts, showing relatively good catalytic activity.

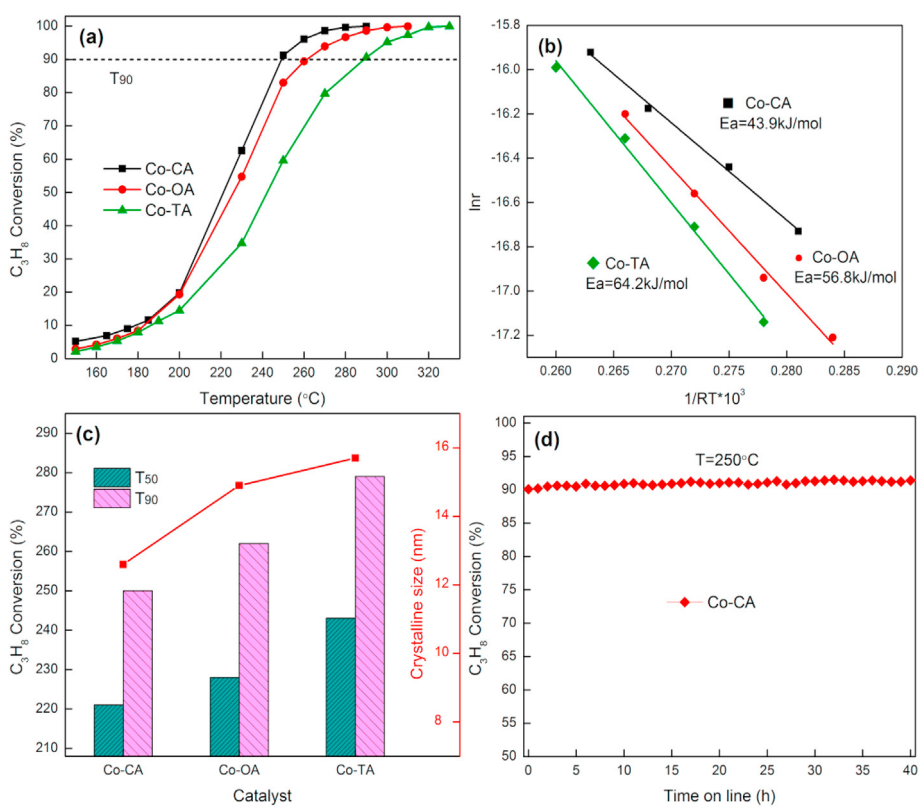

Fig. 11. (a) Catalytic activity of propane combustion; (b) Arrhenius plots of the relationship between ln r and 1/RT; (c) Relationship between crystalline size and catalytic activity (T_{50} and T_{90}); (d) Stability test of Co-CA at 250 °C. Test conditions: The feed consisted of 0.3 vol% propane balanced by air, with a gas hourly space velocity (GHSV) of 30000 mL/(h·g).

Table 5
Comparison with catalysts reported in the literature.

Catalyst	C_3H_8 concentration (ppm)	GHSV ($ml \bullet g^{-1} \bullet h^{-1}$)	T_{90} (°C)	Reference
Co-CA	3000	30000	250	This work
Co_3O_4	3000	12000	280	[61]
Co_3O_4	5000	30000	270	[62]
Co_3O_4	2500	120000	241	[63]
$NiCoO_4$	10000	45000	425	[64]
$MnNiO_x$	2000	30000	242	[65]
$LaMnO_x$	2000	30000	255	[36]
Pt/AlF_3	2000	80000	250	[66]

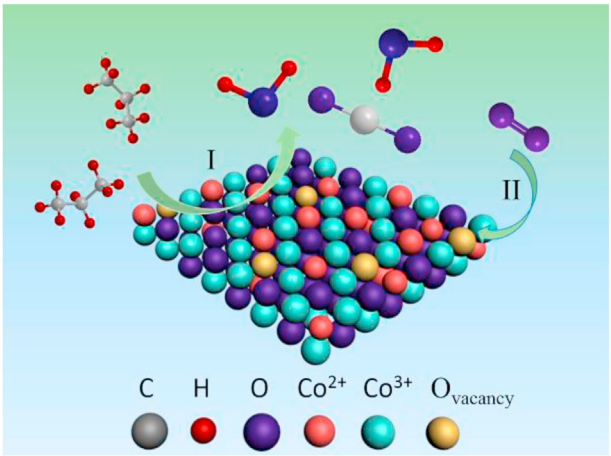

Fig. 12. Schematic of propane oxidation on cobalt oxide.

In situ diffuse reflectance infrared spectroscopy (*in situ* DRIFT) experiments have shown that the deep oxidation of propane on cobalt oxides follows the Mars-van-Krevelen (MVK) mechanism [63,64]. The main reaction process is shown in Fig. 12: In the first step, propane molecules adsorb on the surface of cobalt oxides and react with oxygen atoms attached to metal cations (Co^{2+} and Co^{3+}) to form H_2O, CO_2, and oxygen vacancies. In the second step, the gas phase oxygen molecules are added to the oxygen vacancies, and the metal or metal cations are oxidized. For the Co-CA catalyst, due to the large number of adsorbed oxygen species on its surface, the adsorbed oxygen can be used as active oxygen to participate in the oxidation in the initial reaction. When the adsorbed oxygen is consumed to a certain extent or cannot provide enough active oxygen, the surface lattice oxygen begins to participate in the oxidation. MVK mechanism shows that the lattice oxygen species on the catalyst surface play an important role in the redox reaction. Likewise, this work demonstrates that Co-CA has a distinct surface lattice oxygen desorption peak and the lowest desorption temperature, thus exhibiting excellent catalytic activity. Moreover, the disordered structure and rapid oxygen mobility will generate high-frequency oxygen vacancies, which is conducive to the cycle of the reaction, thereby maintaining stable catalytic activity.

Overall, nanocrystalline Co_3O_4 prepared with CA, OA, and TA as complexing agents has significantly different catalytic performance in catalytic combustion of propane. Co-CA catalyst has the best catalytic activity and excellent stability. FTIR showed that CA, OA, and TA in the catalyst precursor coordinated with Co^{2+} in the form of monodentate, tetradentate, and bidentate, which strongly affected the distance between Co^{2+} ions in catalyst precursor. XRD, N_2 adsorption-desorption, and TEM/HRTEM analysis further indicated that polyhedral nanocrystalline Co_3O_4 were successfully synthesized using different small molecular carboxylic acids, but the crystallite size, texture properties and lattice disorder changed significantly. XPS results indicate that the type of small molecular carboxylic acids has an important effect on the distribution of surface oxygen species and the oxidation state of Co ions. The order of catalytic activity is the same as the order of surface O_{ads}/O_{latt} ratio and Co^{3+}/Co^{2+} ratio, which can be attributed to the abundant Co^{3+} and adsorbed oxygen species on the surface that produce enough active oxygen species to participate in the oxidation reaction. Combined with XPS, O_2-TPD, and H_2-TPR analysis, the surface of the Co-CA has more adsorbed active oxygen species and faster lattice oxygen mobility, resulting in stronger reducibility. These factors contribute to the stronger catalytic oxidation performance of Co-CA than Co-OA and Co-TA.

4. Conclusions

In this work, several nanocrystalline Co_3O_4 catalysts were synthesized based on different small molecular carboxylic acids (citric acid, oxalic acid, and tartaric acid). The effect of small molecular carboxylic acids on the physicochemical properties of the catalyst was discussed in detail, and the catalytic performance for the combustion of propane (a typical short-chain alkane) was evaluated. The results showed that different small molecular carboxylic acids changed the distance between Co^{2+} ions in the catalyst precursor, thus strongly affecting the structure and surface microenvironment of nanocrystalline Co_3O_4. Among them, the nanocrystalline Co_3O_4 synthesized from the cobalt citrate precursor with the largest Co^{2+} ion distance exhibited the best catalytic activity, reaching 90% propane conversion rate at 250 °C, and showed stable performance in 40h continuous reaction. Small crystallite size, high lattice disorder degree, excellent texture properties, abundant surface Co^{3+}, and O_{ads} and strong reducibility are the main reasons for its excellent catalytic performance.

CRediT authorship contribution statement

Zhao Liu: Formal analysis, conducted sample preparation and data analysis. **Lijun Cheng:** Data curation, calculated the data. **Jia Zeng:** Data curation, calculated the data. **Xin Hu:** Data curation, calculated the data. **Shiyun Zhangxue:** Data curation, calculated the data. **Shanliang Yuan:** characterized the samples. **Qifei Bo:** characterized the samples, All authors read and contributed to the manuscript. No conflict of interest exists in the submission of this manuscript, and the manuscript is approved by all authors for publication. **Biao Zhang:** Formal analysis, conducted sample preparation and data analysis. **Yi Jiang:** Formal analysis, conducted sample preparation and data analysis.

Declaration of competing interest

The authors declare that they have no known competing financial interests or personal relationships that could have appeared to influence the work reported in this paper.

Acknowledgements

This work was supported by the Sichuan Science and Technology Program (2018GZ0314) and the "Light of the West" Fund of the Chinese Academy of Sciences.

Appendix A. Supplementary data

Supplementary data to this article can be found online at https://doi.org/10.1016/j.jssc.2020.121712.

References

[1] W. Zhang, J. Díez-Ramírez, P. Anguita, C. Descorme, J.L. Valverde, A. Giroir-Fendler, Nanocrystalline Co_3O_4 catalysts for toluene and propane oxidation: effect of the precipitation agent, Appl. Catal. B Environ. 273 (2020), 118894.
[2] C. He, J. Cheng, X. Zhang, M. Douthwaite, S. Pattisson, Z. Hao, Recent advances in the catalytic oxidation of volatile organic compounds: a review based on pollutant sorts and sources, Chem. Rev. 119 (7) (2019) 4471–4568.

[3] S.R. Ms Kamal, Mm Hossain, Catalytic oxidation of volatile organic compounds (VOCs) A review, Atmos. Environ. 140 (2016) 117–134.
[4] Y.R. Liu, X. Li, W.M. Liao, A.P. Jia, Y.J. Wang, M.F. Luo, J.Q. Lu, Highly active Pt/BN catalysts for propane combustion: the roles of support and reactant-induced evolution of active sites, ACS Catal. 9 (2) (2019) 1472–1481.
[5] C. Rao, C. Peng, H. Peng, L. Zhang, W. Liu, X. Wang, N. Zhang, P. Wu, In situ embedded pseudo Pd–Sn solid solution in micropores silica with remarkable catalytic performance for CO and propane oxidation, ACS Appl. Mater. Interfaces 10 (11) (2018) 9220–9224.
[6] K.A. Ledwa, M. Pawlyta, L. Kępiński, $Ru_xCe_{1-x}O_{2-y}$ nanoparticles deposited on functionalized γ-Al_2O_3 as a thermally stable oxidation catalyst, Appl. Catal. B Environ. 230 (2018) 135–144.
[7] Z. Hu, Z. Wang, Y. Guo, L. Wang, Y. Guo, J. Zhang, W. Zhan, Total oxidation of propane over a Ru/CeO_2 catalyst at low temperature, Environ. Sci. Technol. 52 (16) (2018) 9531–9541.
[8] J. Lei, S. Wang, J. Li, Mesoporous Co_3O_4 derived from Co-MOFs with different morphologies and ligands for toluene catalytic oxidation, Chem. Eng. Sci. 220 (2020), 115654.
[9] J. Zhao, Z. Tang, F. Dong, J. Zhang, Controlled porous hollow Co_3O_4 polyhedral nanocages derived from metal-organic frameworks (MOFs) for toluene catalytic oxidation, Mol Catal 463 (2019) 77–86.
[10] L. Cheng, J. Wang, C. Zhang, B. Jin, Y. Men, Boosting acetone oxidation efficiency over MnO_2 nanorods by tailoring crystal phases, New J. Chem. 43 (48) (2019) 19126–19136.
[11] X. Zhang, H. Zhao, Z. Song, W. Liu, J. Zhao, Z.A. Ma, M. Zhao, Y. Xing, Insight into the effect of oxygen species and Mn chemical valence over MnO on the catalytic oxidation of toluene, Appl. Surf. Sci. 493 (2019) 9–17.
[12] S. Li, Y. Zhang, Z. Wang, W. Du, G. Zhu, Morphological effect of CeO_2 catalysts on their catalytic performance in lean methane combustion, Chem. Lett. 49 (5) (2020) 461–464.
[13] F. Liu, Y. Sang, H. Ma, Z. Li, Z. Gao, Nickel oxide as an effective catalyst for catalytic combustion of methane, J. Nat. Gas Sci. Eng. 41 (2017) 1–6.
[14] X. Zhang, Y. Junhui, Y. Jing, C. Ting, X. Bei, L. Zhe, Z. Kunfeng, Y. Ling, H. Dannong, Excellent low-temperature catalytic performance of nanosheet Co-Mn oxides for total benzene oxidation, Appl. Catal. Gen. 566 (2018) 104–112.
[15] T. Cai, J. Yuan, L. Zhang, L. Yang, Q. Tong, M. Ge, B. Xiao, X. Zhang, K. Zhao, D. He, Ni–Co–O solid solution dispersed nanocrystalline Co_3O_4 as a highly active catalyst for low-temperature propane combustion, Catal Sci Technol 8 (21) (2018) 5416–5427.
[16] Z. Hu, S. Qiu, Y. You, Y. Guo, Y. Guo, L. Wang, W. Zhan, G. Lu, Hydrothermal synthesis of $NiCeO_x$ nanosheets and its application to the total oxidation of propane, Appl. Catal. B Environ. 225 (2018) 110–120.
[17] W. Fang, J. Chen, X. Zhou, J. Chen, Z. Ye, J. Li, Zeolitic imidazolate framework-67-derived CeO_2@Co_3O_4 core–shell microspheres with enhanced catalytic activity toward toluene oxidation, Ind. Eng. Chem. Res. 59 (22) (2020) 10328–10337.
[18] M.H. Mahyuddin, A. Staykov, Y. Shiota, K. Yoshizawa, Direct conversion of methane to methanol by metal-exchanged ZSM-5 zeolite (Metal= Fe, Co, Ni, Cu), ACS Catal. 6 (12) (2016) 8321–8331.
[19] L. Cheng, Z. Liu, S. Yuan, M. Wei, Y. Jiang, Sol–gel citrate procedure to synthesize Ag/Co_3O_4 catalysts with enhanced activity for propane catalytic combustion, Chem. Pap. 74 (5) (2019) 1449–1457.
[20] B. Xiao, K. Zhao, L. Zhang, T. Cai, X. Zhang, Z. Wang, J. Yuan, L. Yang, P. Gao, D. He, A green and facile synthesis of Co_3O_4 monolithic catalyst with enhanced total oxidation of propane performance, Catal. Commun. 116 (2018) 1–4.
[21] Q. Ren, S. Mo, R. Peng, Z. Feng, M. Zhang, L. Chen, M. Fu, J. Wu, D. Ye, Controllable synthesis of 3D hierarchical Co_3O_4 nanocatalysts with various morphologies for the catalytic oxidation of toluene, J. Mater. Chem. 6 (2) (2018) 498–509.
[22] Y. Liu, H. Dai, J. Deng, S. Xie, H. Yang, W. Tan, W. Han, Y. Jiang, G. Guo, Mesoporous Co_3O_4-supported gold nanocatalysts: highly active for the oxidation of carbon monoxide, benzene, toluene, and o-xylene, J. Catal. 309 (2014) 408–418.
[23] V. Iablokov, R. Barbosa, G. Pollefeyt, I. Van Driessche, S. Chenakin, N. Kruse, Catalytic CO oxidation over well-defined cobalt oxide nanoparticles: size-reactivity correlation, ACS Catal. 5 (10) (2015) 5714–5718.
[24] B. Zhao, R. Ran, L. Sun, Z. Yang, X. Wu, D. Weng, A high-surface-area La-Ce-Mn mixed oxide with enhanced activity for CO and C_3H_8 oxidation, Catal. Commun. 105 (2018) 26–30.
[25] Q. Ren, Z. Feng, S. Mo, C. Huang, S. Li, W. Zhang, L. Chen, M. Fu, J. Wu, D. Ye, 1D-Co_3O_4, 2D-Co_3O_4, 3D-Co_3O_4 for catalytic oxidation of toluene, Catal. Today 332 (2019) 160–167.
[26] J. González-Prior, R. López-Fonseca, J.I. Gutiérrez-Ortiz, B. De Rivas, Catalytic removal of chlorinated compounds over ordered mesoporous cobalt oxides synthesised by hard-templating, Appl. Catal. B Environ. 222 (2018) 9–17.
[27] X. Chen, S. a C. Carabineiro, S.S.T. Bastos, P.B. Tavares, J.J.M. rfão, M.F.R. Pereira, J.L. Figueiredo, Exotemplated copper, cobalt, iron, lanthanum and nickel oxides for catalytic oxidation of ethyl acetate, J Environ Chem Eng 1 (4) (2013) 795–804.
[28] T. Baidya, T. Murayama, P. Bera, O.V. Safonova, P. Steiger, N.K. Katiyar, K. Biswas, M. Haruta, Low-temperature CO oxidation over combustion made Fe- and Cr-doped Co_3O_4 catalysts: role of dopant's nature toward achieving superior catalytic activity and stability, J. Phys. Chem. C 121 (28) (2017) 15256–15265.
[29] C. Wang, C. Zhang, W. Hua, Y. Guo, G. Lu, S. Gil, A. Giroir-Fendler, Catalytic oxidation of vinyl chloride emissions over Co-Ce composite oxide catalysts, Chem. Eng. J. 315 (2017) 392–402.
[30] J. Sun, Z. Zhao, Y. Li, X. Yu, L. Zhao, J. Li, Y. Wei, J. Liu, Synthesis and catalytic performance of macroporous $LaCeCoO_3$ perovskite oxide catalysts with high oxygen mobility for catalytic combustion of soot, J. Rare Earths 38 (6) (2020) 584–593.
[31] R. Yang, L. Yu, M. Sun, X. Zhao, G. Cheng, W. Ye, Preparation of 3D micro/nanostructured CeO_2: influence of organic/inorganic acids, Particuology 37 (2018) 17–25.
[32] C. Ren, Z. Zhang, R. Yang, The construction of three-dimensionally ordered macroporous (Fe, Zn, Cu, Co)/$LaMnO_3$ with controllable gelation rate and their catalytic combustion properties, J. Porous Mater. 26 (6) (2019) 1649–1656.
[33] H. Tao, J. Li, Q. Ma, Z. Chen, X. Zhang, Y. Quan, P. Yang, C. Qi, Synthesis of W-Nb-O solid acid for catalytic combustion of low-concentration monochlorobenzene, Chem. Eng. J. 382 (2020), 123045.
[34] M. Zhang, W. Li, X. Wu, F. Zhao, D. Wang, X. Zha, S. Li, H. Liu, Y. Chen, Low-temperature catalytic oxidation of benzene over nanocrystalline Cu–Mn composite oxides by facile sol–gel synthesis, New J. Chem. 44 (6) (2020) 2442–2451.
[35] S. Prasad, A. Vijayalakshmi, N.S. Gajbhiye, Synthesis of ultrafine cobalt ferrite by thermal decomposition of citrate precursor, J. Therm. Anal. Calorim. 52 (2) (1998) 595–607.
[36] Y. Xie, Y. Guo, Y. Guo, L. Wang, W. Zhan, Y. Wang, X.-Q. Gong, G. Lu, A highly-efficient $LaMnO_x$ catalyst for propane combustion: the promotional role of La and the effect of the preparation method, Catal Sci Technol 6 (23) (2016) 8222–8233.
[37] W. Lin, W. Guo, L. Wang, X. Ma, S. Xiang, Z. Zhang, Synthesis, Crystal structure and characterization of a new zinc citrate complex, Chin. J. Struct. Chem. 33 (4) (2014) 591–596.
[38] Y. Deng, X. Xiong, J.P. Zou, L. Deng, M.J. Tu, Control of morphology and structure for β-Co nanoparticles from cobalt oxalate and research on its phase-change mechanism, J. Alloys Compd. 618 (2015) 497–503.
[39] Y. Park, H. Lim, J.-H. Moon, H.-N. Lee, S. Son, H. Kim, H.-J. Kim, High-yield one-pot recovery and characterization of nanostructured cobalt oxalate from spent lithium-ion batteries and successive Re-synthesis of $LiCoO_2$, Metals 7 (8) (2017) 303.
[40] S.R. Suthar, M.J. Joshi, Growth and characterization of Mn^{2+} doped calcium l-tartrate crystals, Cryst. Res. Technol. 41 (7) (2006) 664–670.
[41] S.J. Joshi, K.P. Tank, B.B. Parekh, M.J. Joshi, Characterization of gel grown iron-manganese-cobalt ternary levo-tartrate crystals, Cryst. Res. Technol. 45 (3) (2010) 303–310.
[42] W. Zhang, F. Wu, J. Li, Z. You, Dispersion–precipitation synthesis of highly active nanosized Co_3O_4 for catalytic oxidation of carbon monoxide and propane, Appl. Surf. Sci. 411 (2017) 136–143.
[43] B. Bai, J. Li, Positive effects of K^+ ions on three-dimensional mesoporous Ag/Co_3O_4 catalyst for HCHO oxidation, ACS Catal. 4 (8) (2014) 2753–2762.
[44] W. Wang, H. Qi, H. Long, X. Wang, H. Ru, A simple ternary non-ionic templating system for preparation of complex hierarchically meso–mesoporous silicas with 3D-interconnected large mesopores, J. Mater. Chem. 2 (15) (2014) 5363–5370.
[45] A. Boulaoued, I. Fechete, B. Donnio, M. Bernard, P. Turek, F. Garin, Mo/KIT-6, Fe/KIT-6 and Mo–Fe/KIT-6 as new types of heterogeneous catalysts for the conversion of MCP, Microporous Mesoporous Mater. 155 (2012) 131–142.
[46] W. Tang, W. Xiao, S. Wang, Z. Ren, J. Ding, P.-X. Gao, Boosting catalytic propane oxidation over PGM-free Co_3O_4 nanocrystal aggregates through chemical leaching: a comparative study with Pt and Pd based catalysts, Appl. Catal. B Environ. 226 (2018) 585–595.
[47] B. Bai, H. Arandiyan, J. Li, Comparison of the performance for oxidation of formaldehyde on nano-Co_3O_4, 2D-Co_3O_4, and 3D-Co_3O_4 catalysts, Appl. Catal. B Environ. 142–143 (2013) 677–683.
[48] X. Xie, Y. Li, Z.-Q. Liu, M. Haruta, W. Shen, Low-temperature oxidation of CO catalysed by Co_3O_4 nanorods, Nature 458 (7239) (2009) 746.
[49] C.Y. Ma, Z. Mu, J.J. Li, Y.G. Jin, J. Cheng, G.Q. Lu, Z.P. Hao, S.Z. Qiao, Mesoporous Co_3O_4 and Au/Co_3O_4 catalysts for low-temperature oxidation of trace ethylene, J. Am. Chem. Soc. 132 (8) (2010) 2608–2613.
[50] T. Garcia, S. Agouram, J.F. Sánchez-Royo, R. Murillo, A.M. Mastral, A. Aranda, I. Vázquez, A. Dejoz, B. Solsona, Deep oxidation of volatile organic compounds using ordered cobalt oxides prepared by a nanocasting route, Appl. Catal. Gen. 386 (1–2) (2010) 16–27.
[51] Z. Zhu, G. Lu, Z. Zhang, Y. Guo, Y. Guo, Y. Wang, Highly active and stable Co_3O_4/ZSM-5 catalyst for propane oxidation: effect of the preparation method, ACS Catal. 3 (6) (2013) 1154–1164.
[52] J. Marco, J. Gancedo, M. Gracia, J. Gautier, E. Rios, F. Berry, Characterization of the nickel cobaltite, $NiCo_2O_4$, prepared by several methods: an XRD, XANES, EXAFS, and XPS study, J. Solid State Chem. 153 (1) (2000) 74–81.
[53] X. Li, X. Li, X. Zeng, T. Zhu, Correlation between the physicochemical properties and catalytic performances of micro/mesoporous CoCeO mixed oxides for propane combustion, Appl. Catal. Gen. 572 (2019) 61–70.
[54] S. Rousseau, S. Loridant, P. Delichere, A. Boreave, J. Deloume, P. Vernoux, $La_{(1-x)}Sr_xCo_{1-y}Fe_yO_3$ perovskites prepared by sol–gel method: characterization and relationships with catalytic properties for total oxidation of toluene, Appl. Catal. B Environ. 88 (3–4) (2009) 438–447.
[55] Z. Chen, S. Wang, W. Liu, X. Gao, D. Gao, M. Wang, S. Wang, Morphology-dependent performance of Co_3O_4 via facile and controllable synthesis for methane combustion, Appl. Catal. Gen. 525 (2016) 94–102.
[56] Q. Liu, L.C. Wang, M. Chen, Y. Cao, H.Y. He, K.N. Fan, Dry citrate-precursor synthesized nanocrystalline cobalt oxide as highly active catalyst for total oxidation of propane, J. Catal. 263 (1) (2009) 104–113.
[57] W. Song, A.S. Poyraz, Y. Meng, Z. Ren, S.-Y. Chen, S.L. Suib, Mesoporous Co_3O_4 with controlled porosity: inverse micelle synthesis and high-performance catalytic CO oxidation at −60 °C, Chem. Mater. 26 (15) (2014) 4629–4639.
[58] L. Liotta, M. Ousmane, G. Di Carlo, G. Pantaleo, G. Deganello, G. Marcì, L. Retailleau, A. Giroir-Fendler, Total oxidation of propene at low temperature over Co_3O_4–CeO_2 mixed oxides: role of surface oxygen vacancies and bulk oxygen mobility in the catalytic activity, Appl. Catal. Gen. 347 (1) (2008) 81–88.

[59] W. Si, Y. Wang, S. Zhao, F. Hu, J. Li, A facile method for in situ preparation of the $MnO_2/LaMnO_3$ catalyst for the removal of toluene, Environ. Sci. Technol. 50 (8) (2016) 4572–4578.
[60] B. De Rivas, R. López-Fonseca, C. Jiménez-González, J.I. Gutiérrez-Ortiz, Synthesis, characterisation and catalytic performance of nanocrystalline Co_3O_4 for gas-phase chlorinated VOC abatement, J. Catal. 281 (1) (2011) 88–97.
[61] B. Solsona, T.E. Davies, T. Garcia, I. Vázquez, A. Dejoz, S.H. Taylor, Total oxidation of propane using nanocrystalline cobalt oxide and supported cobalt oxide catalysts, Appl. Catal. B Environ. 84 (1–2) (2008) 176–184.
[62] R.P. Marin, S.A. Kondrat, R.K. Pinnell, T.E. Davies, S. Golunski, J.K. Bartley, G.J. Hutchings, S.H. Taylor, Green preparation of transition metal oxide catalysts using supercritical CO_2 anti-solvent precipitation for the total oxidation of propane, Appl. Catal. B Environ. 140 (Complete) (2013) 671–679.
[63] W. Tang, J. Weng, X. Lu, L. Wen, A. Suburamanian, C.-Y. Nam, P.-X. Gao, Alkali-metal poisoning effect of total CO and propane oxidation over Co_3O_4 nanocatalysts, Appl. Catal. B Environ. 256 (2019), 117859.
[64] Z. Ren, Z. Wu, W. Song, W. Xiao, Y. Guo, J. Ding, S.L. Suib, P.-X. Gao, Low temperature propane oxidation over Co_3O_4 based nano-array catalysts: Ni dopant effect, reaction mechanism and structural stability, Appl. Catal. B Environ. 180 (2016) 150–160.
[65] Y. Xie, Y. Guo, Y. Guo, L. Wang, W. Zhan, Y. Wang, X. Gong, G. Lu, A highly effective Ni-modified MnO_x catalyst for total oxidation of propane: the promotional role of nickel oxide, RSC Adv. 6 (55) (2016) 50228–50237.
[66] X. Li, Y.-R. Liu, W.-M. Liao, A.-P. Jia, Y.-J. Wang, J.-Q. Lu, M.-F. Luo, Synergistic roles of Pt^0 and Pt^{2+} species in propane combustion over high-performance Pt/AlF_3 catalysts, Appl. Surf. Sci. 475 (2019) 524–531.